RESPONSES OF BURIED CORRUGATED METAL PIPES TO EARTHQUAKES

By C. A. Davis[1] and J. P. Bardet,[2] Members, ASCE

ABSTRACT: This study describes the results of field investigations and analyses carried out on 61 corrugated metal pipes (CMP) that were shaken by the 1994 Northridge earthquake. These CMPs, which include 29 small-diameter (below 107 cm) CMPs and 32 large-diameter (above 107 cm) CMPs, are located within a 10 km^2 area encompassing the Van Norman Complex in the Northern San Fernando Valley, in Los Angeles, California. During the Northridge earthquake, ground movements were extensively recorded within the study area. Twenty-eight of the small-diameter CMPs performed well while the 32 large-diameter CMPs underwent performances ranging from no damage to complete collapse. The main cause of damage to the large-diameter CMPs was found to be the large ground strains. Based on this unprecedented data set, the factors controlling the seismic performance of the 32 large-diameter CMPs were identified and framed into a pseudostatic analysis method for evaluating the response of large diameter flexible underground pipes subjected to ground strain. The proposed analysis, which is applicable to transient and permanent strains, is capable of describing the observed performance of large-diameter CMPs during the 1994 Northridge earthquake. It indicates that peak ground velocity is a more reliable parameter for analyzing pipe damage than is peak ground acceleration. Results of this field investigation and analysis are useful for the seismic design and strengthening of flexible buried conduits.

INTRODUCTION

During the 1994 Northridge earthquake, a large-diameter flexible corrugated metal pipe (CMP) collapsed at the Lower San Fernando Dam (LSFD) (Davis and Bardet 1998). One year later, during the 1995 Hyogoken-Nanbu (Kobe) earthquake, the Daikai Subway Station failed in Kobe, Japan (Iida et al. 1996). These two recent failures revealed that we do not fully understand the response of many buried structures to near-field earthquake ground motions.

Before these events, the response of flexible underground structures (e.g., CMP) to earthquakes had not been examined in detail, mainly because there were no reported CMP failures. During postearthquake reconnaissance, CMP culverts are usually not thoroughly inspected, although their damage may lead to multihazard problems to lifelines during subsequent storm flows. Pipe deformation can remain hidden for many months or even years after an earthquake, but can result in the progressive failure of pipes due to erosion, with disastrous and costly effects to supported lifelines. CMPs are commonly assumed to be resistant to strong earthquake effects (e.g., Youd and Beckman 1996) unless subjected to fault displacement and ground movement (e.g., Foundations 1973). This assumption was unsettled by the 1994 Northridge earthquake, when the CMP of the LSFD collapsed and other nearby CMPs were inspected and found to be damaged (Davis and Bardet 1996b).

The design of buried pipes rarely accounts for seismic forces (e.g., Moser 1990), except for differential displacement across a fault (O'Rourke and Trautmann 1980) and transient and permanent axial deformations (*Guidelines* 1984; O'Rourke and Hmadi 1988). Davis and Bardet (1998) presented a simplified pseudostatic analysis based on peak ground accelerations, which explained the failure of the CMP of the LSFD but had some limitations when applied to other types of CMP.

This paper summarizes the result of field investigations on 61 CMPs shaken by the 1994 Northridge earthquake. These investigations were prompted by the scarcity of case histories and methods of analysis on the response of CMPs to strong near-field earthquakes. Based on these case histories, a simplified strain-based analysis is proposed to identify the parameters controlling the seismic performance of CMPs and is compared with the previously proposed acceleration-based analysis. These case studies and the companion analysis are intended to help engineers improve methods for designing new buried structures and strengthening existing ones.

CHARACTERISTICS OF CMPS UNDER STUDY

Fig. 1 shows the location of the 61 CMPs identified in this study. They are located within a 10 km^2 area encompassing the Los Angeles Department of Water and Power's (LADWP) Van Norman Complex (VNC). The VNC is a critical lifeline facility that provides water and power to the City of Los Angeles. It is also one of the closest sites to the 1994 ruptured fault surface (Bardet and Davis 1996a).

The CMPs were arbitrarily subdivided into two categories —29 small diameter (below 107 cm) and 32 large diameter (above 107 cm). They were inspected intermittently from 1994 through 1997, depending on accessibility. Fig. 2(a) shows the distribution of CMP by size and degree of inspection. All small CMP were circular. Only one small CMP was damaged during the Northridge earthquake, as a result of corrosion deterioration prior to the earthquake. Therefore our observations imply that the current methods of analysis using static loads (e.g., Standard 1992) provide an adequate factor of safety for small CMP to sustain strong seismic ground motion. Hereafter, only the 32 large-diameter CMPs will be examined.

Fig. 2(c) shows the span distribution for large diameter CMPs defined in Fig. 3, which range from 107 to 478 cm. Table 1 summarizes their function, age, shape, and earthquake performance. The pipes are identified with a number (i.e., Pipe 5). When the pipe characteristics change along their length, additional letters are used to identify pipe segments (e.g., Pipe 5E and 5W). As shown in Fig. 3, CMPs were divided into five subsets—circular, elliptical, circular arch, pipe arch, and underpass—according to their cross-sectional shape (*Standard* 1992). Fig. 2(b) shows the distribution of the cross-sectional shapes in Fig. 3, the properties of which are summarized in Tables 2–4. The characteristics listed in Tables 1–4 were obtained from field inspections and measurements; they were supplemented with design and construction drawings when those were available. All of the pipes were made of galvanized steel, and except for Pipes 5, 6, and 26, all were fabricated in accordance with ASTM A 444. The drainage slopes were less than 10% on all pipes except for some portions of Pipes 3,

[1]Geotech. Engr., Dept. of Water and Power, Los Angeles, CA.
[2]Prof., Civ. Engrg. Dept., Univ. of Southern California, Los Angeles, CA.

Note. Discussion open until June 1, 2000. To extend the closing date one month, a written request must be filed with the ASCE Manager of Journals. The manuscript for this paper was submitted for review and possible publication on October 23, 1998. This paper is part of the ***Journal of Geotechnical and Geoenvironmental Engineering***, Vol. 126, No. 1, January, 2000. ©ASCE, ISSN 1090-0241/00/0001-0028–0039/$8.00 + $.50 per page. Paper No. 19524.

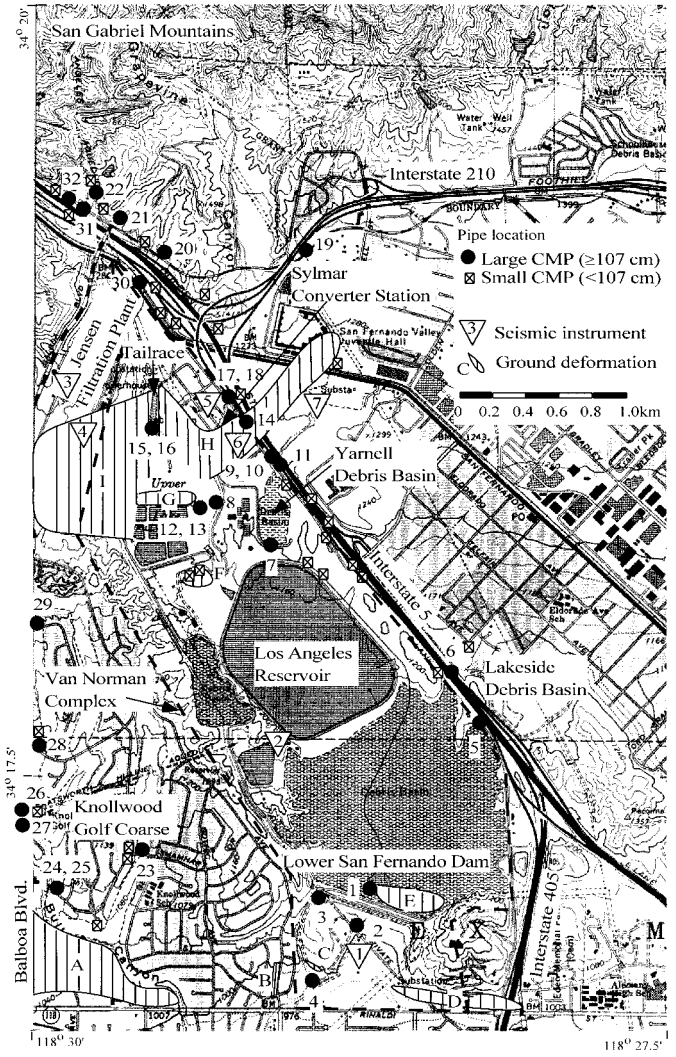

FIG. 1. Study Area Including Van Norman Complex, Locations of Large and Small CMP, Strong Motion Instruments, and Regions of Observed Permanent Ground Deformation

26, and 27, which had 40, 15, and 23% slopes, respectively. Corrosion damage was observable only in Pipe 26; therefore, corrosion was not a factor controlling the performance of the large-diameter pipes under study. All pipes were backfilled with soil, except for Pipes 15 and 16, which were encased in concrete.

As shown in Tables 2–4, the pipes are designated as single-plate or multiplate. Single-plate pipes have individual pipe segments, which are shop-fabricated with a single corrugated sheet welded or riveted along its axial and circumferential seams. The pipe segments are connected in the field. Multiplate pipes are made of multiple corrugated sheets, which are formed in the shop and bolted together in the field. In contrast to single-plate pipes, their cross section consists of multiple curved plates. Each pipe segment is assembled by bolting the curved plates together at a spacing of half the pitch length. The segments are connected with bolts around the pipe circumference. Bolt connections are usually offset on adjoining segments.

Tables 2–4 list relevant geotechnical parameters, including the maximum depth of fill above the pipe, foundation material, average shear wave velocity C_s, and depth to ground water. The construction methods, type, and method of fill placement were not investigated in detail except for Pipes 1–4 (Davis and Bardet 1996b). CMPs under Interstate 5 (I-5), I-405, and I-210 were probably placed according to AASHTO standards. Foundation materials were determined from local geological descriptions from the LADWP and geological maps (e.g., Dibblee 1991). Alluvium consists of sand, silt, or clay mixtures. Bedrock consists mainly of weak sedimentary sandstone and siltstone rocks of various formations. The average shear wave velocities in the upper 30 m were estimated at each pipe location from measurements compiled in Bardet and Davis (1996a,c) and Gibbs et al. (1996). Ground-water levels were noted only with respect to elevation of the pipe invert during the 1994 Northridge earthquake. Ground-water elevations vary with rainfalls, and the exact levels for all pipe locations was not known during the 1994 Northridge earthquake. In this study, it was sufficient to determine only whether the pipes were above or below the water table.

GROUND MOTION AND DEFORMATION DURING NORTHRIDGE QUAKE

Transient Ground Motions

Nineteen instruments in the VNC recorded the 1994 Northridge earthquake's main shock. Fig. 1 and Table 5 show the locations, peak accelerations, and peak velocities of seven strong motion instruments. As described by Bardet and Davis (1996a), the intensity of the near-field ground motions varied spatially and directionally around the VNC. Figs. 4 and 5 show traces of recorded accelerations and velocities in the north-south (N-S) and east-west (E-W) directions projected in the horizontal and vertical planes. The recordings in Figs. 4 and 5 and Table 5 are representative of the variation of strong ground motion in the study area.

The VNC is located above the northern end and right in line with the slip direction of the fault that ruptured in the 1994 Northridge earthquake. As a result, it was subjected to strong near-source pulses (Bardet and Davis 1996a). As pointed out by Somerville and Graves (1993), the intensity of near-field shaking depends on the structure location and orientation with respect to the direction of fault rupture. As shown in Figs. 4 and 5, the recorded horizontal ground motion was generally strongest in the N-S direction (direction of slip) and varied largely with azimuth. Similarly, the motions varied with di-

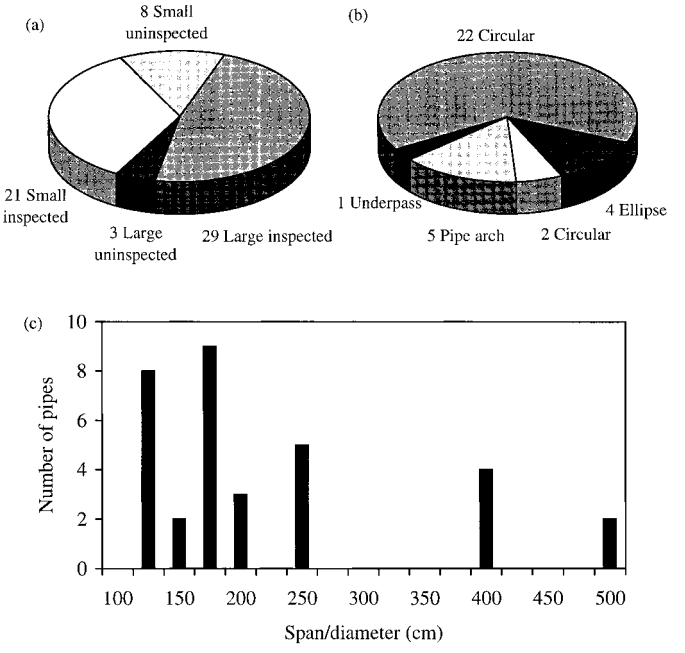

FIG. 2. Distribution of Various CMP Observations: (a) Number of Large- and Small-Diameter CMPs Identified and Inspected; (b) Number of Large-Diameter CMPs by Cross-Sectional Shape; (c) Number of Large-Diameter CMPs by Span

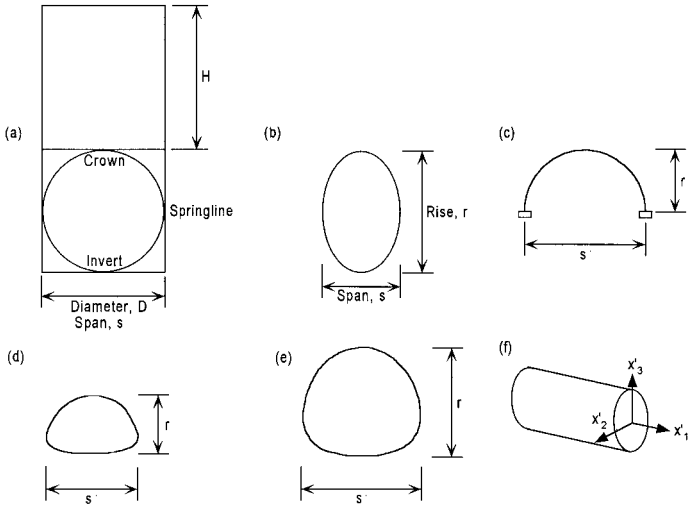

FIG. 3. Cross-Sectional Shapes and Orientation of 32 Large-Diameter CMPs Studied: (a) Circular Pipe; (b) Elliptical; (c) Circular Arch; (d) Pipe Arch; (e) Underpass; and (f) Axes Orientation

rections in the vertical plane. This implies that the pipes in the present study were subjected to various intensities of transverse shaking depending on their orientation.

The longitudinal, transverse, and vertical axes of the strong motion recordings are denoted x_1, x_2, and x_3, respectively. The x_1- and x_2-axes are both horizontal, with positive orientation in the northern and eastern directions, respectively. The positive x_3-axis is pointing upward. In this coordinate system, the components of accelerations and velocities are a_i and v_i (i = 1, 2, 3). Table 5 summarizes the peak ground accelerations and velocities in the x_{12}-plane and along the x_3-axis. The ground motions parallel to the longitudinal axes of individual pipes were calculated by rotating accelerations and velocities from the x_1-axes to the x_1'-axis, which are defined in Fig. 3(f). The corresponding azimuth values of the x_1'-axis are given for each pipe in Tables 2–4. Figs. 6(a and b) summarize the absolute peak accelerations pga_1 and pga_{32} along the x_1'-axis and in the x_{32}'-plane, respectively, for the strong motion recordings of Fig. 4. Figs. 6(c and d) summarize the absolute peak velocities pgv_1 and pgv_2 along the x_1' and x_2'-axes, respectively, for the strong motion recordings shown in Fig. 5. The vertical component of ground velocity is practically negligible, as shown in Fig. 5. The range of peak ground acceleration and velocity in Fig. 6 was estimated for each pipe from the recordings at the closest stations and those with the most similar soil conditions.

As shown in Table 5, Stations 1 to 7 recorded ground motions on a variety of soil conditions. The shear wave velocities C_s reported in Table 5 were measured at each recording site (Gibbs et al. 1996; Bardet and Davis 1996c). Stations 2, 3, and 7 were located on bedrock, Stations 1 and 5 on relatively firm alluvial soils, and Stations 4 and 6 on weak soils that exhibited nonlinear response during the 1994 Northridge earthquake (Cultrera et al. 1998). Table 5 and Fig. 6 show a wide range of peak accelerations and velocities over short distances, even for similar soil conditions. This variation renders difficult the selection of a particular ground motion recording for analyzing a pipe. Therefore, all analyses were carried out with the range of ground motions shown in Fig. 6.

Permanent Ground Deformation

Fig. 1 shows the nine areas where permanent ground deformation was observed around the VNC following the 1994 Northridge earthquake. The ground deformations in these areas, designated by letters A through I, are attributed to the failures of surficial soils and not to deeper fault movement. Areas A through I represent regions of large permanent deformation. The area boundaries in Fig. 1 were identified by observation of ground cracks and significant damage to buried and surface structures that were clearly related to permanent ground movements. In this study, the amplitudes of permanent ground strain were not measured in details as in O'Rourke and Hamada (1992). Only the permanent strains that were observable on the ground surface have been considered.

The ground deformations in areas A–D are described by Hart et al. (1995) and Hecker et al. (1995). In area A, which extends over 0.5 km^2, the horizontal ground deformations were the largest; they reached 60 cm (Hecker et al. 1995). These deformations ruptured numerous gas and water pipe lines on Balboa Blvd. (O'Rourke and O'Rourke 1995). No CMP were identified in Area A. In areas B and C, deformations were smaller; they were caused by lateral soil movements along tributary stream channels. Areas B and C were near Pipe 4, but there was no evidence of lateral ground deformations in the immediate vicinity of Pipe 4. Surface cracks were observed above Pipe 4 but were attributed to pipe deformations and not ground deformations at B and C. In area D, the ground deformations, which took place in a preexisting landslide at the base of the Mission Hills (Hecker et al. 1995), did not damage any underground structures. In area E, extensive ground deformation resulted from the liquefaction of saturated hydraulic fill upstream of the LSFD (Bardet and Davis 1996b). These deformations were generally in the north-northeasterly direction. Pipe 1 suffered extensive lateral buckling along the westerly boundary of area E. However, as shown in Davis and Bardet (1998), the failure of Pipe 1 could not be solely attributed to the liquefaction of hydraulic fills, because most of Pipe 1 segments failed within nonliquefiable bedrock and alluvium. In areas F and G, ground movements damaged two large water distribution lines (Davis and Bardet 1995) but did not affect any large CMPs. Two small-diameter CMPs located near the center of area F remained undamaged, mainly because they were very short and moved as rigid blocks with the ground around them.

In areas H and I, which were the largest of all areas, the ground deformations were marked by settlement and lateral movement, and they caused soil cracks and breaks in buried water pipes and concrete channels. These deformations were gravity-driven in westerly and easterly directions, respectively, and were not continuously distributed across the regions outlined in Fig. 1 (Davis and Bardet 1995). Ground deformations in region H caused some cracking in the road adjacent to Pipe 14 and some damage to the coating inside the pipe. At the convergence of areas H and I, the Tailrace was severely damaged (Davis and Bardet 1996a). However, Pipes 15 and 16 were encased in concrete and suffered only minor distortions.

In summary, there were nine regions of ground deformation documented within the study area, three of which influenced the performance of four large diameter pipes.

CMP PERFORMANCE DURING NORTHRIDGE QUAKE

Table 1 summarizes the seismic performance and quality of inspection for the large CMP under study. The inspection quality was classified in four categories:

A. The pipe interior was entered and thoroughly inspected without obstruction.
B. The pipe interior was inspected by partially entering the interior, and was observed from end to end.
C. The pipe interior was only partially inspected from one end, but was neither entered nor observed from end to end.

TABLE 1. Location, General Information, and Earthquake Performance of Large-Diameter Corrugated Metal Pipes Under Study

Pipe (1)	Location (2)	Function (3)	Year placed (4)	Shape (5)	Northridge earthquake performance (6)	Inspection quality (7)	Comments (8)
1	Lower San Fernando Dam, drain line #1	drainage culvert/outlet line	1973	circular	lateral collapse	A	(Davis and Bardet 1998)
2	Lower San Fernando Dam, drain line #1	drainage culvert/outlet line	1973	circular	no damage	A	
3	Lower San Fernando Dam, drain line #2	drainage culvert/outlet line	1973	circular	no damage	A	
4	San Fernando and Bull Creek channels	drainage culvert	1973	circular	lateral and axial deformation	A	
5W 5E	Lakeside Debris Basin under I-5/I-405 interchange	drainage culvert	1950's/1960	circular	lateral and axial deformation	A	Older pipe under I-405 (lateral and axial deformation) connected to newer pipe to east under I-5 (no damage); 1971 headwall damage.
6W 6E	Lakeside storm channel under I-5	drainage culvert	1950's/1960	circular	no damage	A	1971 headwall damage; Filled in to springline elevation before 1971
7	Yarnell Debris Basin outlet	drainage culvert/outlet line	1962	elliptical	no damage	B	Circular pipe having 5% elongation to form elliptical shape
8	Backwash ponds, pump station	drainage culvert	1986	circular	no damage	B	Tar coated
9, 10	Yarnell Debris Basin inlet	drainage culverts	1960	arch	no damage	A	
11	Yarnell Debris Basin inlet, I-5 drainage	drainage culvert	1950's/1960	circular	no damage	B	Pipe extended west in 1960
12, 13	Backwash ponds	drainage culverts	1986	circular	no damage	B	
14	Sylmar Converter Station parallel to Sepulveda Blvd.	drainage culvert	after 1971	circular	lateral displacement	A	Tar coating damaged from lateral soil movements
15, 16	Tailrace outlet	aqueduct channel discharge	1940	circular	no significant damage	A	Concrete encased; Founded on liquefiable soil, dike failed on east side of pipes
17W 18W	Sylmar Converter Station under Sepulveda Blvd.	drainage culverts	1968	elliptical	no damage/minor deformation	A	Circular pipe having 5% elongation Connect to Pipes 17E and 18E
17E 18E	Sylmar Converter Station under Sepulveda Blvd.	drainage culverts	1950's	circular	no damage/minor deformation	A	Connect to Pipes 17W and 18W to the west and concrete pipes under I-5 to the east
19	Foothill Blvd. and I-210	drainage culvert	1953	circular	no apparent damage	C	
20	Foothill Blvd./I-5 south of L.A. aqueduct	drainage culvert	1967	circular	no apparent damage	C	
21	Foothill Blvd./I-5 south of L.A. aqueduct	drainage culvert	1967	elliptical	no apparent damage	C	Circular pipe having 5% elongation to form elliptical shape
22	Los Angeles Aqueduct cascades	drainage culvert	1970	circular	vertical deformation	B	Deformation probably occurred after construction but enhanced by earthquake
23	Knollwood Golf Course at Shamhart Dr.	pedestrian culvert	before 1971	arch	lateral deformation	A	Deformation suspected to exist prior to earthquake
24, 25	Knollwood Golf Course at Knollwood Dr.	drainage culverts	before 1971	arch	no damage	A	
26	Bull Creek at Balboa Blvd.	drainage culvert	1956	circular	failure of corroded invert	A	Pre-earthquake corrosion damage Sinkholes appeared in road 11 months after earthquake
27	Chatsworth High Line at Balboa Blvd.	pipe encasement	1956	underpass	no damage	C	
28	Knollwood Golf Course at Pineridge Dr.	pedestrian culvert	before 1971	circular arch	no damage	A	
29	Knollwood Golf Course at Culven Dr.	pedestrian culvert	before 1971	circular arch	no damage	A	
30A 30B	Under I-5, parallel to freeway	drainage culvert	1967	circular	not verified	D	Series of 107 cm and 122 cm diameter pipes
31	Under I-5, west of L.A. aqueduct cascades	drainage culvert	1967	circular	not verified	D	
32	Under I-5, west of L.A. aqueduct cascades	drainage culvert	1967	circular	not verified	D	

TABLE 2. Properties of Large-Diameter Circular Corrugated Metal Pipes under Study

Pipe (1)	Diameter *D* (cm) (2)	Azimuth (degrees) (3)	Length (m) (4)	Thickness (mm) (5)	Corrugation			Single or Multiplate structure (9)	Segment length (m) (10)	Joint connection (11)	Seam connection (12)	Maximum fill depth (m) (13)	Foundation material (14)	Shear wave velocity C_s (m/s) (15)	Ground water depth from invert (16)
					Pitch (cm) (6)	Depth (cm) (7)	Annular or Helical (8)								
1	244	12, 42	116	4.27	6.8	1.3	A	S	7.3	strap	welded	11.9	alluv./BR	400–500	2.4 m above
2	152	148–241	219	3.51	6.8	1.3	H	S	7.3	strap	welded	2.4	alluvium	450	below
3	152	165–195	123	3.51	6.8	1.3	H	S	7.3	strap	welded	5.5	bedrock	500	below
4	244	54	31	4.27	6.8	1.3	A	S	7.3	welded	welded	2.1	alluvium	350	at
5W	381	50	45	4.78	15.2	3.81	A	M	3.05	bolted	bolted	9.7	alluvium	350	below
5E	381	50	96	5.54	15.2	5.1	A	M	2.43	bolted	bolted	9.7	alluvium	350	below
6W	381	2	61	5.54	15.2	3.81	A	M	3.05	bolted	bolted	7	bedrock	450	below
6E	381	8	81	5.54	15.2	5.1	A	M	2.43	bolted	bolted	7	bedrock	450	below
8	152	45	73	3.51	6.8	1.3	A	S	7.3	strap	welded	1	alluvium	600	at
11	152	15	52	3.51	6.8	1.6	A	S	7.3	riveted	strap	3	alluvium	500	at
12, 13	122	0	14.6	3.51	6.8	1.3	H	S	7.3	strap	welded	1	alluv./fill	350	0.3 m above
14	198	142	256	3.51	6.8	1.9	H	S	7.3	strap	welded	0.6	alluvium	250–300	below
15, 16	152	5	19	3.51	6.8	1.6	A	S	7.3	concrete	welded	5.5	alluvium	400	above pipe
17, 18E	198	20	34	4.27	6.8	1.3	A	S	7.3	strap	riveted	3.4	alluvium	350	below
19	152	60	152	3.51	6.8	1.3	A	S	2.7	—	riveted	7.6	alluvium	500	at
20	122	25	196	4.27	6.8	1.3	A	S	7.3	strap	riveted	6.1	alluvium	600	unknown
22	152	15	106	3.51	6.8	1.3	A	S	2.7	strap	welded	3	bedrock	600	0.3 m above
26	244	160	105	4.26	15.2	5.1	A	M	2.4	bolted	bolted	9	alluv./fill	550	below
30A	107	130	54	3.51	6.8	1.3	A	S	7.3	strap	—	0.9	alluvium	400	below
30B	122	140	141	3.51	6.8	1.3	A	S	7.3	strap	—	0.6	alluvium	400	below
31	168	30–155	232	2.77	6.8	1.3	A	S	7.3	strap	—	13.1	bedrock	600	below
32	107	30	172	2.77	6.8	1.3	A	S	7.3	strap	—	3	bedrock	600	below

TABLE 3. Properties of Large-Diameter Elliptical Corrugated Metal Pipes under Study

Pipe (1)	Span *s* (cm) (2)	Rise *r* (cm) (3)	Azimuth (degrees) (4)	Length (m) (5)	Thickness (mm) (6)	Corrugation			Single or Multiplate structure (10)	Segment length (m) (11)	Joint connection (12)	Seam connection (13)	Maximum fill depth (m) (14)	Foundation material (15)	Shear wave velocity C_s (m/s) (16)	Ground water depth from invert (17)
						Pitch (cm) (7)	Depth (cm) (8)	Annular or Helical (9)								
7	114	132	0	64	3.51	6.8	1.3	A	S	7.3	riveted/ slip	riveted	10	bedrock	600	at/below
17, 18W	183	213	20–120	31	4.27	6.8	1.3	A	S	7.3	strap	riveted	3.4	alluvium	350	below
21	107	130	35, 60, 90	103	2.77	6.8	1.3	H	S	3.05	strap	welded	13.7	alluv./BR	600	below

TABLE 4. Properties of Large-Diameter Arch and Underpass Corrugated Metal Pipes under Study

Pipe (1)	Diameter/span *s* (cm) (2)	Rise *r* (cm) (3)	Azimuth (degrees) (4)	Length (m) (5)	Thickness (mm) (6)	Corrugation			Single or Multiplate structure (10)	Segment length (m) (11)	Joint connection (12)	Seam connection (13)	Maximum fill depth (m) (14)	Foundation material (15)	Shear wave velocity C_s (m/s) (16)	Ground water depth from invert (17)
						Pitch (cm) (7)	Depth (cm) (8)	Annular or Helical (9)								
9, 10	221	160	15	90	3.51	15.2	5.1	A	M	2.4	bolted	bolted	2.5	alluvium	500	at
23	391	244	5	24.7	4.76	15.2	5.1	A	M	2.9	bolted	bolted	3	alluvium	550	below
24, 25	127	79	45	12	1.62	6.8	1.3	A	S	3.05	riveted	riveted	1	alluvium	550	below
27	376	366	80	25	4.76	15.2	5.1	A	M	2.7	bolted	bolted	3.6	fill	550	below
28	477.5	477.5	30	15.2	4.76	15.2	5.1	A	M	3.05	bolted	bolted	0.5	alluvium	550	below
29	477.5	477.5	155	15.2	4.76	15.2	5.1	A	M	3.05	bolted	bolted	0.5	alluvium	550	below

D. The pipe location was identified in the field but could not be inspected.

Most pipes showed signs of either transient or permanent deflections. The effects of transient motions were mainly noticeable at pipe joints where the ends of loosely connected segments came temporarily into contact or bolted connections had slipped during the earthquake shaking. These transient deformations were clearly identifiable by markings in the pipe coating. In addition to transient deformations, a few pipes sustained permanent deformations. In some cases pipe segments impacted each other with enough force to leave small local deformations, while the cross-sectional shapes of others were significantly distorted. Since there were no preearthquake measurements made on any CMPs, it was difficult to determine whether small transverse distortions preexisted or resulted from the earthquake. Consequently, small deformations that left the pipe structurally intact are not reported in Table 1. As shown in Fig. 7 and Table 1, six CMPs (i.e., 1, 4, 5, 14, 22, and 26) underwent five forms of damage and significant deformation after the 1994 Northridge earthquake. Prior to that earthquake, Pipes 1, 4, 5, and 14 were in good operating condition but Pipe 22 had deformed vertically and Pipe 26 was corroded. Pipe 22 had a deflected shape similar to pipes embedded in poorly compacted soils (Moser 1990). The joints of Pipes 15 and 16 partially separated because of beam-type bending caused by foundation and embankment deformations. However, the concrete surrounding these pipes remained intact and largely contributed to their good performance. As noted in Table 1, there was no evidence that Pipe 23 deformed because of the Northridge earthquake. The pipes that could not be accessed or thoroughly inspected (i.e., quality C and D) were considered to be undamaged based on the absence of (1) reported damage from local highway officials (Youd and Beckman 1996) and (2) surface deformations above these pipes. However, the lack of reported or surficial evidence is not con-

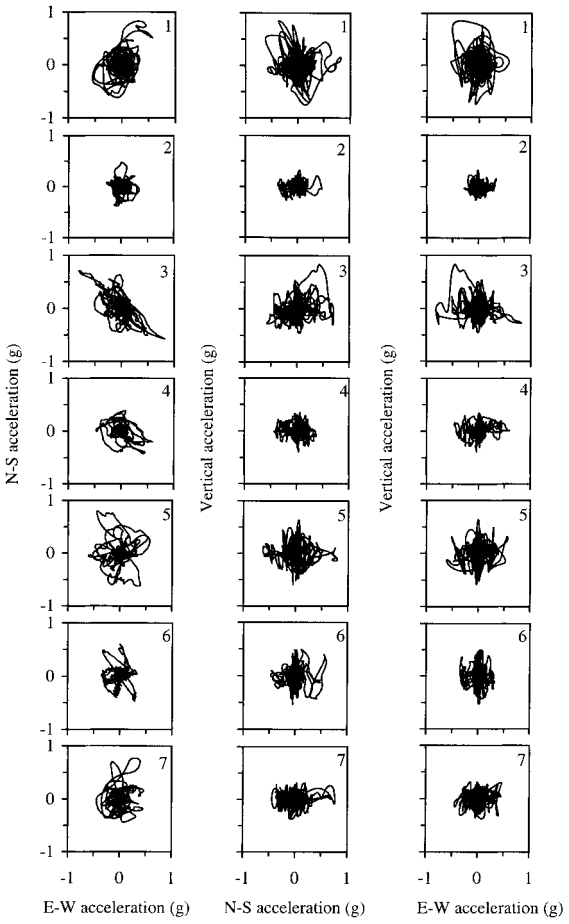

FIG. 4. Traces of Acceleration in Horizontal and Vertical Planes Recorded at Seven Stations during 1994 Northridge Earthquake (Refer to Table 5 and Fig. 1 for Station Identification)

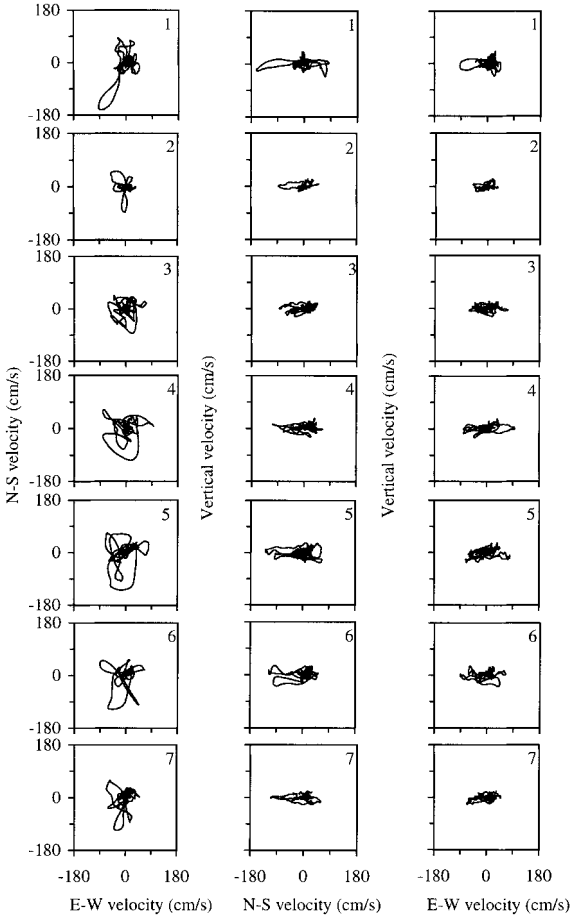

FIG. 5. Traces of Velocity in Horizontal and Vertical Planes Recorded at Seven Stations during 1994 Northridge Earthquake (Refer to Table 5 and Fig. 1 for Station Identification)

clusive evidence for the absence of damage. For example, damage to Pipes 5 and 26 was not discovered for over a year after the 1994 earthquake.

Figs. 8(a–c) show damaged sections of Pipes 1, 4, and 5, respectively—results of the 1994 earthquake. Pipe 1 suffered complete lateral collapse. Pipe 4 sustained transverse deformations measuring up to 14 cm. Eleven 19-mm diameter bolts were sheared along the spring line of Pipe 5W, which allowed 10 cm of lateral separation and 6.4 cm of vertical shortening. In addition, as shown in Fig. 8(c), the diameter of Pipe 5 was permanently distorted by up to 20 cm along a 18 m length. Longitudinal buckling also occurred in Pipes 4 and 5, whereas no axial deformations were observed on Pipe 1. As a result of limited soil movement, damage to Pipe 14 was more superficial than structural, causing minor deformations of the shell and spalling of the tar coating. Vertical deflection of Pipe 22 existed prior to the Northridge earthquake and was enhanced by settlement of the embedding soils during shaking. Buckling of Pipe 26 was clearly related to severe corrosion of the invert.

ANALYSIS OF CMP DAMAGE

Detailed site investigations were performed with the goal of identifying parameters influencing the seismic response of CMPs. The investigation results are summarized in Tables 1–4. Fig. 7 shows that six large-diameter CMPs (19%) were damaged during the 1994 Northridge earthquake. Based on the CMP data set collected after the earthquake, the factors controlling CMP performance were classified in three main categories: (1) not a cause of damage; (2) cause of damage; and (3) potential causes of damage needing further investigation.

Causes of Damage

Five potential factors of damage to CMPs did not apply to the 32 large diameter CMP data set: (1) fault displacement; (2) pipe foundation failure; (3) standard manufacturing methods; (4) standard construction methods; and (5) drainage slope. There was no evidence of fault movement or soil foundation failure that could have lead to CMP damage. Manufacturing and construction factors were ruled out as damage causes because all the pipes—except for Pipes 5W, 6W, 22, and 26—were manufactured and constructed to similar standards (e.g., *Standard* 1992; ASTM A 760 and A 798); this was verified in detail for Pipes 1 to 4 (Davis and Bardet 1996b). For the range of pipe inclination in Tables 2–4, there was no indication that the pipe drainage slope affected CMP performance.

Three other factors were identified as particular sources of damage to Pipes 14, 22, and 26, respectively: (1) permanent ground deformation; (2) settlement of poorly compacted embedding soils (construction method not meeting current standards); and (3) corrosion. In contrast, causes of damage to Pipes 1, 4, and 5 were not readily apparent from the field investigations.

The factors controlling CMP performance that need further investigation were identified as follows: (1) strain amplitude from transient ground motions and permanent ground deformation; (2) orientation of pipe relative to ground motion direction; (3) pore pressure buildup within the embedding soils; (4) stiffness reduction of embedding soils; (5) soil-pipe relative stiffness; (6) cross-sectional shape; (7) depth of burial and preearthquake static hoop stress; (8) joint and seam connections; and (9) combination of longitudinal and lateral deformations. The most significant factors were difficult to identify

TABLE 5. Peak Ground Accelerations and Velocities Recorded at Van Norman Complex during 1994 Northridge Earthquake

Station (1)	Location (2)	Foundation (3)	Shear wave velocity C_s (m/s) (4)	Peak Ground Acceleration (g)					Peak Ground Velocity (cm/s)				
				pga_1 N-S (5)	pga_2 E-W (6)	pga_3 up (7)	pga_{12} (8)	Azimuth θ_{12} (degree) (9)	pgv_1 N-S (10)	pgv_2 E-W (11)	pgv_3 up (12)	pgv_{12} (13)	Azimuth θ_{12} (degree) (14)
1	Rinaldi Receiving Station	alluvium	350	0.82	0.57	0.85	0.90	25	−162	−94	−42	184	209
2	Los Angeles Dam abutment	bedrock	650	0.48	0.35	0.32	0.48	90	−86	−51	26	86	182
3	Jensen Filtration Plant Generator building	bedrock	600	0.71	0.82	0.83	1.08	311	−84	72	−27	87	164
4	Administration building	alluv./fill	425	−0.43	0.60	−0.39	0.63	109	−108	96	35	109	169
	Sylmar Converter Station												
5	Valve group 7 free-field	alluvium	300	0.80	−0.61	0.64	0.91	331	−129	80	34	130	190
6	Valve group 1–6 basement	alluvium	250	0.60	−0.35	−0.53	0.60	0	−116	−90	−38	128	207
7	Sylmar Converter Station East FF	bedrock	500	0.77	0.47	−0.38	0.84	25	−111	−67	−24	116	199

based on the field investigations alone. Some factors may have combined on some pipes, and acted separately with different intensity on others. For example, Davis and Bardet (1998) concluded that axial deformation did not influence the buckling of Pipe 1. On the other hand, field investigations indicate that the damage to Pipes 4 and 5 may have been influenced by the combination of longitudinal and transverse loads. Field measurements alone were unable to show whether the transverse deformations at Pipes 4 and 5 resulted from the direct application of axial forces or from the initiation of a transverse buckling mode. In addition, it is not clear if the connections failed on Pipe 5 from an increase in transverse loads, axial loads, or from large deformations initiated from transverse buckling. Timoshenko and Woinowsky-Krieger (1970) noted that an analytical solution for axial deformations in CMP is difficult to obtain and generally cannot be readily applied in solving practical problems as those described herein. In view of the problem complexity, simplified analyses for transverse buckling of circular flexible pipe were developed to identify the relative importance of different parameters. The pipes may have also been influenced by other limiting conditions such as yielding of the base metal and development of a plastic hinge. A single limit state does not apply to all the pipes under study; for example, Pipes 22 and 26 were damaged from excessive deflection and corrosion, respectively. However, the permanent transverse deformations noted on Pipes 1, 4, and 5 indicate that buckling may have been the critical limiting condition. Preliminary calculations showed that the yield capacity of Pipes 1 and 4 was greater than their buckling resistance and was approximately the same for Pipe 5. Duncan (1979) noted the buckling resistance of CMP having large flexural stiffness is usually greater than their yield strength. However, the buckling strength is a function of soil stiffness (Moore 1989), which decreases with the intensity of seismic shaking (Seed and Idriss 1970). Therefore, to identify the factors causing damage to Pipes 1, 4, and 5, this report focuses on transverse buckling deformations, leaving the effects of longitudinal deformations, yielding, plastic hinges, and seam connections for further study.

Static Analysis

The examination of the CMPs stability under static gravity loading alone is helpful not only for understanding the preearthquake conditions but also for formulating the seismic analysis. The static analysis consists of (1) evaluating the pipe load and calculating the resulting maximum hoop force per unit length N, then (2) examining if the pipe can resist that load by comparing N with the critical hoop force N_{cr}. The factor of safety FS against failure is

$$FS = \frac{N_{cr}}{N} = \frac{\varepsilon_{cr}}{\varepsilon_v} \tag{1}$$

where ε_v = applied hoop strain; $\varepsilon_{cr} = N_{cr}/AE_p$ = critical hoop strain at buckling; A = cross-sectional area of the pipe shell; and E_p = pipe Young's modulus. Both ε_v and ε_{cr} are defined with respect to the undeformed area A. The maximum hoop force per unit length N is (Moser 1990)

$$N = \frac{F_v}{2} \tag{2}$$

where F_v = vertical resultant force acting on the top of pipe. The vertical and horizontal pipe strains, ε_v and ε_h, are determined from

$$\varepsilon_v = \frac{F_v}{2AE_p} \text{ and } \varepsilon_h = \frac{F_h}{2AE_p} \tag{3}$$

where F_h = horizontal resultant force acting on the pipe.

The maximum hoop force in a flexible buried conduit is difficult to determine because of various factors, including trench geometry, compaction effects, variation of soil properties around the pipe, soil-pipe interaction, effect of sloping ground, and arching effects. Such approximate methods as the limit equilibrium method of Marston (Spangler and Handy 1982; Moser 1990) or the elastic closed-form solution of Burns and Richard (1964) give a first-order approximation of the hoop force in the pipe. These methods can be used to calculate the load applied to the pipe in terms of a dimensionless arching factor β:

$$\beta = \frac{F_v}{\rho g H D} \tag{4}$$

where ρ = soil density; g = acceleration of gravity; H = depth of fill over the pipe; and D = pipe diameter. As recommended by Moser (1990), β is assumed equal to 1. However, β may be slightly higher or lower than 1 for CMP, depending on the pipe stiffness, method of analysis, and assumptions made. Fig. 9(a) shows the static hoop force per unit length N on each pipe calculated for the depth of fill presented in Tables 2–4. Pipes 15 and 16 are encased in concrete and do not behave as flexible conduits. They are included in the analysis only for comparative purposes. There are two load conditions for Pipe 1 labeled as 1S and 1N, representing the different fill depths on the north and south ends.

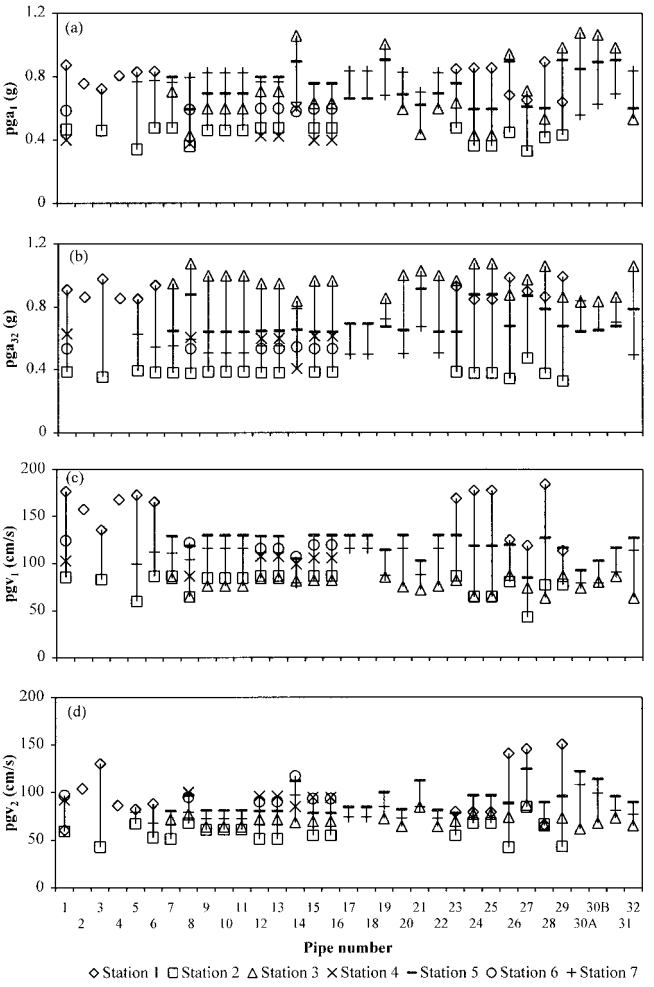

FIG. 6. Projected Components of Absolute Peak Ground Acceleration and Velocity Recorded at Seven Strong Motion Stations: (a) Longitudinal Peak Ground Acceleration pga_1; (b) Transverse Peak Ground Acceleration pga_{23}; (c) Longitudinal Peak Velocity pgv_1; and (d) Transverse Horizontal Peak Ground Velocity pgv_2

The critical hoop force per unit length for buckling is determined from an elastic continuum model for the soil around the pipe (Moore 1989):

$$N_{cr} = 0.66(E_p I)^{1/3} \left(\frac{E_s}{1 - \nu_s^2}\right)^{2/3} \quad (5)$$

where I = pipe moment of inertia; E_s = soil Young's modulus; and ν_s = soil Poisson ratio. In this analysis E_p, E_s, and ν_s were taken as 200 GPa, 12.4 MPa, and 0.3, respectively, for all the pipes. For standard sections, the values of A and I were obtained from ASTM A 796 using the properties from Tables 2–4. Pipes 5W, 6W, and 26 are nonstandard and their section properties were estimated. Shallow cover may reduce the pipes buckling resistance (Moore et al. 1994); however, no adjustments were made for the shallow pipes under study, because either their stiffnesses were sufficiently large as to render the shallow effects negligible (e.g., Pipe 29) or the static soil loading was negligible (e.g., Pipe 14).

E_s increases with depth of burial, degree of compaction, and age, and therefore will vary slightly from pipe to pipe. However, E_s was assumed to be the same for all pipes for direct comparison purpose. Except for Pipes 15 and 16, which are encased in concrete, this is a reasonable assumption in view of the similarities in pipe construction (e.g., Standard 1992; ASTM A 798). The value of E_s = 12.4 MPa was estimated by assuming that the native soils (consisting of sandy silts, silty sands, and clayey sands) were placed around the pipes with reasonable compaction. This value of E_s is a lower bound for sandy soils and an intermediate-to-high value for compacted silty soils (Bardet 1997), but may not adequately represent the poorly compacted soils around Pipe 22.

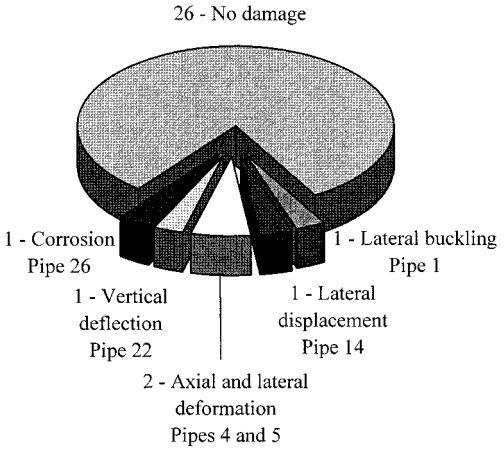

FIG. 7. Distribution of Observed Damage from 1994 Northridge Earthquake

Fig. 9(b) shows the calculated static factors of safety FS against buckling for all the 32 large-diameter pipes. For all pipes FS is greater than 2. As shown in Fig. 9(b), FS becomes very large for some shallow pipes and even exceeds 100 in some cases. These large values are expected because our calculations account only for the fill overburden, and they neglect the surcharges and traffic loads that were used in the original design of these pipes. In conclusion, all CMPs were stable under static soil loads.

Strain-Based Analysis

The proposed analysis consists of determining the changes in applied hoop force per unit length N and critical hoop force per unit length N_{cr} relative to static conditions, which are generated by permanent and/or transient ground strains resulting from earthquakes. The change in hoop force results from the shear and compressional strains, whereas the reduction in N_{cr} originate from modulus reduction and pore pressure increases in the soil around the pipe due to shaking. As shown in Fig. 10, the strain state within the square soil element ABCD surrounding the pipe is assumed uniform. In theory, the strain can originate from transient or permanent ground movements. However, for the present CMP data set, ground strain originated mainly from transient ground motion. The transient shear strain γ is evaluated as follows:

$$\gamma = \frac{v_2}{C_s} \quad (6)$$

where v_2 = horizontal particle velocity transverse to the pipe, and C_s = average shear wave velocity in soil element ABCD. The transient vertical strain ε_{vd} is

$$\varepsilon_{vd} = \frac{v_3}{C_p} \quad (7)$$

where C_p = compression wave velocity, and v_3 = vertical particle velocity. The transient horizontal strain ε_{hd} is considered negligible by assuming that increases in lateral pressures around restrained underground structures result mainly from shearing distortions. When there is no slippage at the soil-pipe interface, the strains in the pipe coincide with those in the surrounding soil. Therefore, γ and ε_{vd} can be superimposed with ε_v and ε_h. Using the Mohr representation of strain (e.g., Bardet 1997), one can determine the direction for which the

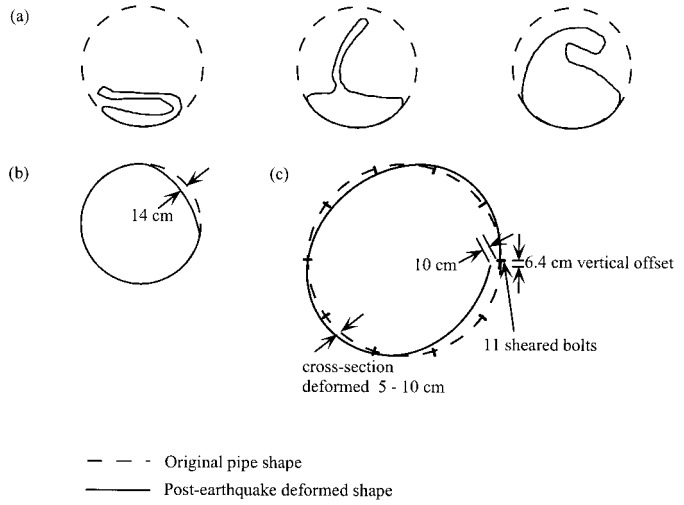

FIG. 8. Deformed CMP Shapes: (a) Pipe 1; (b) Pipe 4; and (c) Pipe 5

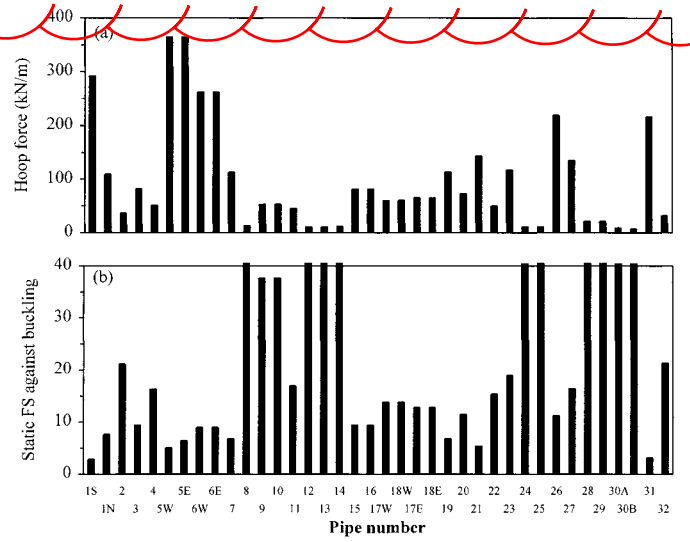

FIG. 9. Results of Static Analysis: (a) Estimated Hoop Force for Arching Factor β = 1; (b) Estimated Static Factor of Safety *FS* against Buckling

shear strain γ is zero and the normal strain is maximum (i.e., $\varepsilon = \varepsilon_{max}$). This case corresponds to the maximum principal strain:

$$\varepsilon_{max} = \frac{1}{2}(\varepsilon_v + \varepsilon_{vd} + \varepsilon_h) + \sqrt{\frac{1}{4}(\varepsilon_v + \varepsilon_{vd} - \varepsilon_h)^2 + \left(\frac{1}{2}\gamma\right)^2} \quad (8)$$

Because the pipes are flexible, $v_3 << v_2$, and $C_p >> C_s$, one may assume $\varepsilon_v = \varepsilon_h$ and $\varepsilon_{vd} << \gamma$. Therefore (8) becomes

$$\varepsilon_{max} = \frac{F_{max}}{2AE_p} = \varepsilon_v + \frac{\gamma_{max}}{2} \quad (9)$$

where F_{max} = maximum normal applied force, and γ_{max} = peak ground shear strain in (6). When the pipe fails under dynamic loads, F_{max} is equal to $2N^d_{cr}$, where N^d_{cr} is the critical hoop force per unit length under dynamic conditions, which can be related to its static counterpart N_{cr} through the dimensionless coefficient X:

$$X = \frac{N^d_{cr}}{N_{cr}} = \frac{F_{max}}{F_v FS}, \quad (10)$$

from which

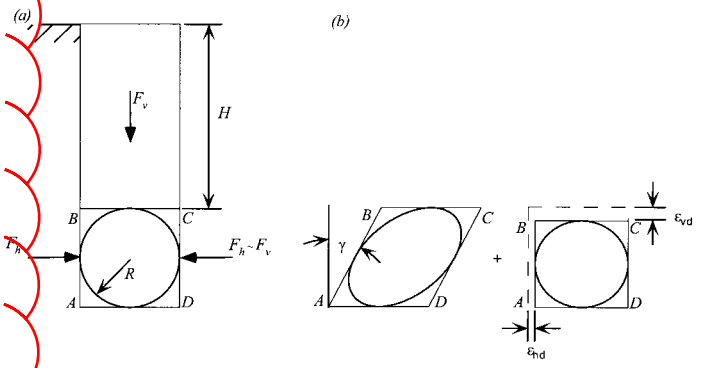

FIG. 10. Diagrams for Strain-Based Analysis: (a) Static Forces Applied to Buried Pipes; and (b) Shear and Vertical Strain Induced by Ground Movements

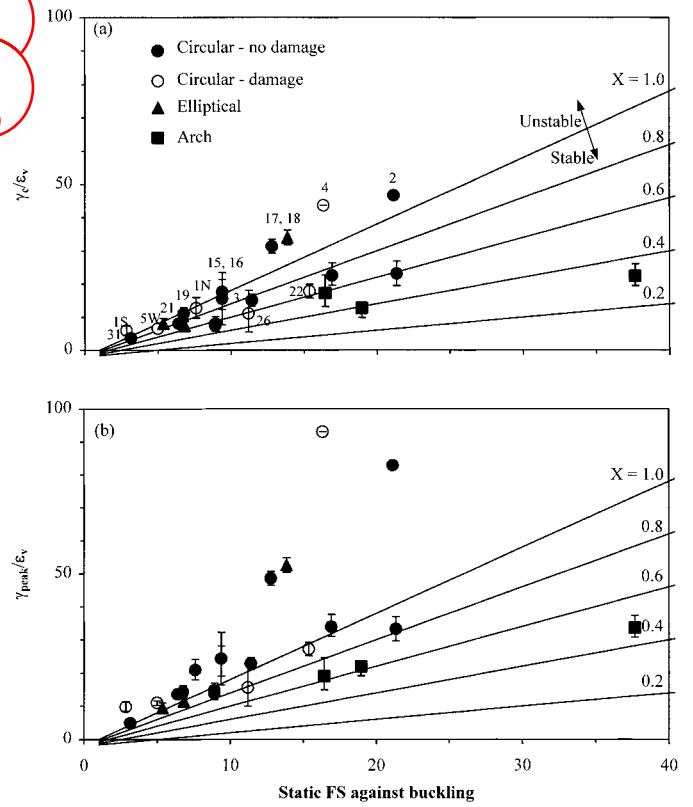

FIG. 11. Results of Strain-Based Analysis for Large-Diameter Pipes for β = 1 and Shear Strain Calculated Using (a) Transverse Peak Ground Velocity (*pgv*$_2$); and (b) Horizontal Peak Ground Velocity (*pgv*$_{12}$)

$$\varepsilon_{max} = X\varepsilon_v FS \quad (11)$$

After introducing the critical shear strain γ_c at the onset of failure, (9) and (11) give the following relation:

$$\frac{\gamma_c}{\varepsilon_v} = 2(XFS - 1) \quad (12)$$

Eq. (12) defines the critical ground strain γ_c required to fail a pipe having a static hoop strain ε_v and static safety factor *FS*. The strain ratio γ_c/ε_v increases linearly with *X* and *FS*. *X* can be evaluated in terms of soil moduli by noting that the critical hoop force per unit length N_{cr} is related to Young's modulus through (5). *X* can also be related to the ratio of excess pore pressure by assuming that Young's modulus is proportional to the square root of mean effective stress (Seed and Idriss 1970; Bardet 1997). Therefore *X* can be expressed as follows:

$$X = \left(\frac{E}{E_s}\right)^{2/3} \approx \left(1 - \frac{\Delta u}{\sigma'_0}\right)^{1/3} \quad (13)$$

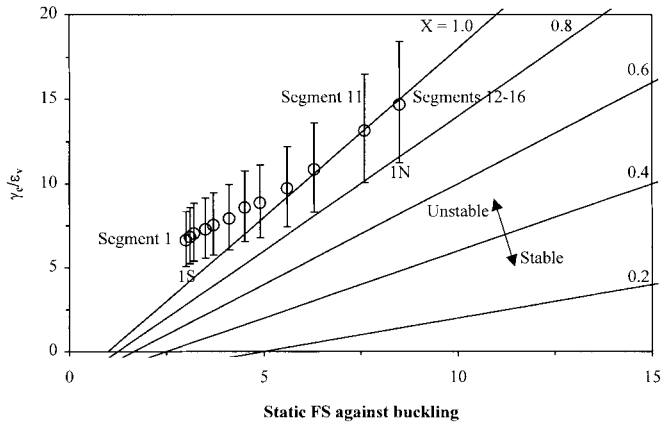

FIG. 12. Results of Strain-Based Analysis for 16 Separate Segments of Pipe 1

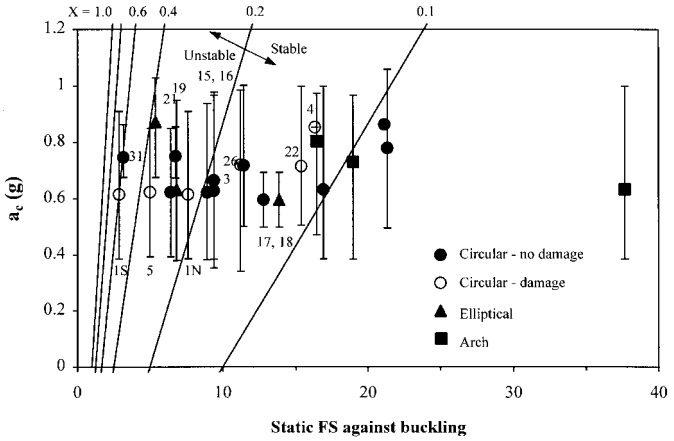

FIG. 13. Results of Acceleration-Based Analysis for Large-Diameter Pipes

where E = soil Young's modulus during cyclic strain loading and E_s = static Young's modulus used in (5); σ_0' = vertical effective stress; and Δu = pore water pressure generated during cyclic loading. Eq. (13) assumes the Poisson's ratio of the embedding soils is the same under static and dynamic loading conditions.

Fig. 11(a) shows the minimum strain ratio required to cause buckling for values of X ranging from 1 to 0.2. Fig. 11(a) also shows the range of strain ratios calculated for each pipe from (3) and (6) with the range of pgv_2 values shown in Fig. 6(d). For a given value of X, the pipe is stable when the point (FS, γ_c/ε_v) is below the straight line defined in (12) and unstable above that line. Although the analysis strictly applies only to circular sections, elliptical and arch sections are included in Fig. 11 for comparative purposes. The FS for some shallow buried pipes are beyond the scale provided in Fig. 11. Fig. 11(a) predicts the buckling of Pipes 1S and 4 during the 1994 Northridge earthquake, without the need for a reduction in buckling strength (i.e., X = 1). In addition, with a slight reduction in buckling strength (i.e., X = 0.8 to 0.9), Fig. 11(a) predicts the buckling of Pipes 1N and 5W. At the same time, Fig. 11(a) indicates that Pipes 2, 3, 17E, 18E, 19, 21, and 31 were to buckle during the earthquake. Fig. 11(a) also shows that Pipes 22 and 26 may not have been damaged if they were properly constructed and maintained and that Pipes 15 and 16, which were submerged below the ground water, may have suffered significant damage if they were not concrete encased. Variation between actual and predicted performance is expected considering that the conditions for each pipe have been approximated in the analysis. Changes in stiffness of the underlying and embedding soils can provide significant changes in the results of Fig. 11(a). In addition, the analysis is sensitive to the orientation of the pipe with respect to the direction of fault rupture. This directional effect is clearly demonstrated by comparing the buckling analysis results of Figs. 11(a and b). In Fig. 11(a), γ_c was determined from pgv_2, the peak velocity oriented transverse to the pipe, whereas in Fig. 11(b), γ_{peak} was calculated from pgv_{12}, the peak ground velocity in the horizontal plane. As shown in Fig. 5, pgv_2 varies with azimuth while pgv_{12} occurs at a particular angle θ_{12}. The use of pgv_2 results in a good correlation with the field performance, whereas the use of pgv_{12} indicates that most all the pipes had to buckle. Table 5 shows that θ_{12} varied across the VNC by as much as 45°, which can significantly influence the analysis results. For example, a 10° variation of θ_{12}, such as that between Stations 5 and 7, could reduce the results of Pipes 17W and 18W by 21%, which is enough to lower the points (FS, γ_c/ε_v) in Fig. 11(a) near the X = 1 line. The analyses presented herein estimate an upper-bound hoop force because they assume no slippage at the soil-pipe interface. Interface slippage could reduce the forces within the pipe.

Fig. 12 shows the range of strain ratios for each individual segment of Pipe 1. The pipe segments, which are numbered from 1 to 16, undergo changes in static loads due to the change in fill depth above Pipe 1 (Davis and Bardet 1998). Segment 1 corresponds to Pipe 1A in Fig. 11, and segments 12–16 correspond to Pipe 1N in Fig. 11. As shown in Fig. 12, it is possible to conclude that segments 1 to 6 failed for X = 1 during the Northridge earthquake. For other segments to fail, only a slight reduction in E was necessary during dynamic loading (i.e., 0.8 < X < 1). This reduction may have been caused by the buildup of pore pressure in the embedding material, without the need for complete liquefaction (i.e., X = 0), or by the modulus degradation with strain of unsaturated embedding soils. Fig. 12 implies that the strain-based analysis can be applied not only to pipes as a whole but also to individual segments along the pipe length.

The strain-based analysis indicates that the large transient velocities recorded in the VNC damaged Pipes 1, 4, and 5 and that permanent ground strains were not necessary for damage to occur. Combining these results with Pipe 14, it is concluded that the main cause of damage to large-diameter CMP is large ground strain resulting from transient and/or permanent ground deformation.

Comparison with Acceleration-Based Analysis

Davis and Bardet (1998) previously analyzed the transverse buckling of Pipe 1 using a pseudostatic force method based on peak ground acceleration. This method, which was initially developed to understand the performance of Pipe 1 alone, is reexamined for the data set of 32 large-diameter CMPs. This analysis is an extension of previous independent analyses that considered only vertical acceleration (Davis and Bardet 1996b,c; Byrne et al. 1996). The critical acceleration a_c required to buckle a pipe is evaluated in terms of the static factor of safety FS, arching factor β, and dimensionless coefficient X as follows (Davis and Bardet 1998):

$$\frac{a_c}{g} = \frac{\beta}{2}\sqrt{4 - \beta^2}\,(XFS - 1) \tag{14}$$

The coefficient X is defined in (13). The critical peak ground acceleration a_c increases linearly with FS and X, and depends nonlinearly on β. A pipe having a static FS value becomes unstable if pga_{32} exceeds a_c. Fig. 13 shows the values of a_c required for buckling at β = 1 and X ranging from 1 to 0.1. For a given value of β and X, a pipe is stable when the point (FS, a_c) is below the straight line defined in (14), and unstable above it.

Fig. 13 also represents the results of the acceleration-based analysis for the large CMP, previously analyzed using the strain-based method. The values of *FS* are identical to those in Fig. 11. The range of acceleration a_c, which is represented by vertical bars in Fig. 13, is calculated based on the range of peak ground accelerations pga_{32} in Fig. 6(b). pga_{32} represents the maximum acceleration in the vertical plane (i.e., the vector sum of horizontal and vertical acceleration). Fig. 13 implies that Pipe 1 could have failed during the 1994 Northridge earthquake with a small reduction in the stiffness of the embedding soil, which could have resulted from partial pore pressure buildup without a complete liquefaction. This analysis conclusion is in agreement with the detailed field observations in Davis and Bardet (1997). However, Fig. 13 also implies that no pipe could have failed during the Northridge earthquake without a reduction in coefficient *X*, which is not in agreement with all the field observations. Fig. 13 can only explain the observed buckling of Pipes 1N, 4, and 5 by a reduction in *X* during dynamic loading (i.e., $X < 1$). Indeed, *X* must be less than 0.1 for Pipe 4 to fail, which implies the almost complete loss of soil stiffness that is associated with soil liquefaction. However, liquefaction did not occur for Pipe 4, since there was no water around Pipe 4. Davis and Bardet (1996b,c) previously showed that the forces generated by the peak vertical ground accelerations alone are not sufficient to collapse Pipe 1. It is therefore concluded that the acceleration-based analysis may not be adequate for analyzing all types of flexible pipes under various conditions, and that the peak ground velocity used in the strain-based analysis [i.e., (12)] provides a more reliable prediction of pipe performance.

DISCUSSION

This study provides data and analysis useful for understanding the damage to buried flexible pipes during earthquakes. However, this investigation applies only to the failure of pipes due to ground movement, and makes no attempt to calculate the amplitude of pipe deformation. The lack of soil properties and measurements of pipe geometry prior to the 1994 Northridge earthquake precludes more detailed analyses.

Based on the field data, no conclusions can be reached as to the influence of different cross-sectional shapes on seismic performance. There was also no distinguishable difference in performance between single plate and multiplate structures. As shown in Fig. 11(a), only two noncircular pipes (17W and 18W) underwent conditions leading to buckling.

The effects of pore water pressure on pipe stability could not be evaluated thoroughly based on the present data set, because during the 1994 Northridge earthquake, Pipe 1 was the only CMP not encased in concrete submerged below the groundwater.

Corrosion was the only factor causing damage to one of the 29 small CMPs studied. In contrast, small-diameter flexible pipes were damaged by transverse loading during the 1995 Kobe earthquake (Tohda et al. 1996). The difference in performance during the two earthquakes warrants a more detailed evaluation of the seismic performance of small flexible pipes.

This investigation has identified a number of areas in need of further research, including (1) axial deformation of pipes with flexible connections; (2) dynamic soil-pipe interaction and buckling; (3) the effects of soil-pipe interface; (5) better documentation of preearthquake pipe conditions; and (5) the effects of pore pressure increases.

CONCLUSIONS

The seismic performance of underground corrugated metal pipes (CMP) have been investigated based on the observed responses of 61 CMPs to the 1994 Northridge earthquake. These case studies demonstrate that 28 out of 29 small-diameter CMPs all performed well during the earthquake (corrosion being the only damaging factor to one small CMP), but that 32 large-diameter flexible buried pipes responded differently to strong ground motions. These case studies also point out that significant CMP damage can occur but still be unobservable at the ground surface, emphasizing the need for postearthquake inspections of critical pipes. Based on these case studies, the factors controlling the seismic performance of CMPs were identified and framed in a simplified strain-based pseudostatic analysis. The comparison of the strain-based analysis with the previously proposed acceleration-based analysis (Davis and Bardet 1998) suggests that transient ground velocity is a more reliable index of CMP damage than is acceleration. The strain-based analysis is capable of explaining the observed performance of 32 large-diameter CMPs during the 1994 Northridge earthquake. The analysis can also be used for the design of new pipes and strengthening of existing pipes subjected to transient or permanent ground movements.

ACKNOWLEDGMENTS

C. Zadorian and T. Kilmer, of the City of Los Angeles Department of Public Works, and J. Payfer and E. Limon, Department of Sanitation, provided information on Pipe 26. P. Scantlin and P. Lahr of the Los Angeles Department of Water and Power assisted in some field inspections. The writers acknowledge the contributions of the Los Angeles Department of Water and Power. The writers also thank J. Chen for preparing figures.

APPENDIX. REFERENCES

Bardet, J. P. (1997). *Experimental soil mechanics*. Prentice-Hall, Upper Saddle River, N.J.

Bardet, J. P., and Davis, C. A. (1996a). ''Engineering observations on ground motion at the Van Norman Complex after the Northridge earthquake.'' *Bull. Seismolog. Soc. Am.*—Special Northridge Issue, 86(1B), S333–S349.

Bardet, J. P., and Davis, C. A. (1996b). ''Performance of San Fernando dams during the 1994 Northridge earthquake.'' *J. Geotech. and Geoenvir. Engrg.*, ASCE, 122(7), 554–564.

Bardet, J. P., and Davis, C. A. (1996c). ''Study of near-source ground motion at the Van Norman Complex after the 1994 Northridge earthquake.'' *Proc., Workshop on Site Response Subjected to Strong Ground Motions*, Port and Harbour Research Institute, Yokosuka, Japan, 2, 1–13.

Burns, J. Q., and Richard, R. M. (1964). ''Attenuation of stress for buried cylinders.'' *Proc., Symp. on Soil Struct. Interaction*, University of Arizona, Tucson, Ariz., 378–392.

Byrne, P. M., Anderson, D. L., and Jitno, H. (1996). ''Seismic analysis of large buried culvert structures.'' *Transp. Res. Rec.*, 1541, 133–139.

Cultrera, G., Boore, D. M., Joyner, W. B., and Dietel, C. M. (1999). ''Nonlinear soil response in the vicinity of the Van Norman Complex following the 1994 Northridge, California, earthquake.'' *Bull. Seismolog. Soc. Am.*, 89(5).

Davis, C. A., and Bardet, J. P. (1995). ''Seismic performance of Van Norman water lifelines.'' *Proc., 4th U.S. Conf. on Lifeline Earthquake Engrg.*, San Francsico, ASCE, New York, 652–659.

Davis, C. A., and Bardet, J. P. (1996a). ''Performance of two reservoirs during 1994 Northridge earthquake.'' *J. Geotech. and Geoenvir. Engrg.*, ASCE, 122(8), 613–622.

Davis, C. A., and Bardet, J. P. (1996b). ''Performance of four corrugated metal pipes during the 1994 Northridge earthquake.'' *Proc., 6th Japan-U.S. Workshop on Earthquake-Resistant Design of Lifeline Facilities and Countermeasures against Soil Liquefaction*, M. Hamada and T. D. O'Rourke, eds., National Center for Earthquake Engineering Research, Buffalo, N.Y., 77–93.

Davis, C. A., and Bardet, J. P. (1996c). ''Failure of a buried corrugated metal pipe during the 1994 Northridge earthquake.'' *Proc., 11th World Conf. on Earthquake Engrg.*, Mexico, Elsevier Science, Amsterdam.

Davis, C. A., and Bardet, J. P. (1998). ''Seismic analysis of large diameter flexible underground pipes.'' *J. Geotech. and Geoenvir. Engrg.*, ASCE, 124(10), 1005–1015.

Dibblee, T. W. Jr. (1991). ''Geologic map of the San Fernando and Van Nuys (North 1/2) quadrangles.'' *Map #DF-33*, Dibblee Geologic Foundation.

Duncan, J. M. (1979). ''Behavior and design of long-span metal culverts.'' *J. Geotech. Engrg. Div.*, ASCE, 105(3), 399–418.
Foundations Section, California Division of Highways. (1973). ''Earthquake damage to California highways.'' Utilities, Transportation and Sociological Aspects, Vol. II of ''San Fernando, California, Earthquake of February 9, 1971,'' U.S. Dept. of Commerce, *NOAA Spec. Rep.*, 235–246.
Gibbs, J. F., Tinsley, J. C., and Joyner, W. B. (1996). ''Seismic velocities and geological conditions at twelve sites subjected to strong ground motion in the 1994 Northridge, California, earthquake.'' *Open-File Rep. 96-740*, U.S. Geological Survey, Washington, D.C.
Guidelines for the seismic design of oil and gas pipeline systems. (1984). Committee on Gas and Liquid Fuel Lifelines, ASCE, New York.
Hart, E. W., Treiman, J. A., and Bryant, W. A. (1995). ''The search for fault rupture after the Northridge earthquake.'' *The Northridge, California, earthquake of 17 January 1994*, M. C. Woods and W. R. Seiple, eds., California Department of Conservation, Div. of Mines and Geology, Special Publ. 116, 89–101.
Hecker, S., Ponti, D. J., Garvin, C. D., and Hamilton, J. C. (1995). ''Characteristics and origin of ground deformation produced in Granada Hills and Mission Hills during the January 17, 1994 Northridge, California, earthquake,'' *The Northridge, California, Earthquake of 17 January 1994*, M. C. Woods and W. R. Seiple, eds., California Department of Conservation, Div. of Mines and Geology, Special Publ. 116, 111–131.
Iida, H., Hiroto, T., Yoshida, N., and Iwafuji, M. (1996). ''Damage to Daikai subway station.'' *Soils and Found.*, Special Issue on Geotechnical Aspects of the January 17, 1995, Hyogoken-Nambu Earthquake, Japanese Geotechnical Society, 283–300.
Moore, I. D. (1989). ''Elastic buckling of buried flexible tubes—a review of theory and experiment.'' *J. Geotech. Engrg.*, ASCE, 115(3), 340–358.
Moore, I. D., Haggag, A., and Selig, E. T. (1994). ''Buckling strength of flexible cylinders with non-uniform elastic support.'' *Solids and Struct.*, 31(22), 3041–3058.
Moser, A. P. (1990). *Buried pipe design*. McGraw-Hill, New York.
O'Rourke, M. J., and Hmadi, K. E. (1988). ''Analysis of continuous buried pipelines for seismic wave effects.''*Earthquake Engrg. and Struct. Dyn.*, 16, 917–929.
O'Rourke, T. D., and Trautmann, C. H. (1980). ''Analytical modeling of buried pipeline response to permanent earthquake displacements.'' *Geotech. Engrg. Rep. 80-4*, School of Civil and Environmental Engineering, Cornell University, Ithaca, N.Y.
O'Rourke, T. D., and O'Rourke, M. J. (1995). ''Pipeline response to permanent ground deformation: A benchmark case.'' *Proc., 4th U.S. Conf. on Lifeline Earthquake Engrg.*, San Francisco, ASCE, New York, 288–295.
O'Rourke, T. D., and Hamada, M., eds. (1992). ''Case studies of liquefaction and lifeline performance during past earthquakes.'' *Rep. NCEER-92-0002*, Vol. 2, National Center for Earthquake Engineering Research, Buffalo, N.Y.
Somerville, P., and Graves, R. (1993). ''Conditions that give rise to unusually large long period ground motions.'' *The structural design of tall buildings*, Vol. 2, 211–232.
Spangler, M. G., and Handy, R. L. (1982). *Soil engineering*, 4th Ed., Harper and Row, New York.
Standard specifications for highway bridges. (1992). American Association of State Highway and Transportation Officials (AASHTO), Washington, D.C.
Timoshenko, S. P., and Woinowsky-Krieger, S. (1970). *Theory of plates and shells*, 2nd Ed., McGraw-Hill, Auckland, New Zealand.
Tohda, J., Yoshimura, H., and Li, L. (1996). ''Characteristic features of damage to the public sewerage systems in the Hanshin Area.'' *Soils and Found.*, Special Issue on Geotechnical Aspects of the January 17, 1995, Hyogoken-Nambu Earthquake, Japanese Geotechnical Society, 335–347.
Youd, T. L., and Beckman, C. J. (1996). ''Highway culvert performance during earthquakes.'' *Rep. NCEER-95-0016*, National Center for Earthquake Engineering Research, Buffalo, N.Y.